Wang et al. Nanoscale Research Letters (2015) 10:135
DOI 10.1186/s11671-015-0846-y

Nanoscale Research Letters
a SpringerOpen Journal

NANO EXPRESS Open Access

Excellent resistive switching properties of atomic layer-deposited $Al_2O_3/HfO_2/Al_2O_3$ trilayer structures for non-volatile memory applications

Lai-Guo Wang[1,2], Xu Qian[1], Yan-Qiang Cao[1], Zheng-Yi Cao[1], Guo-Yong Fang[1], Ai-Dong Li[1*] and Di Wu[1]

Abstract

We have demonstrated a flexible resistive random access memory unit with trilayer structure by atomic layer deposition (ALD). The device unit is composed of $Al_2O_3/HfO_2/Al_2O_3$-based functional stacks on TiN-coated Si substrate. The cross-sectional HRTEM image and XPS depth profile of $Al_2O_3/HfO_2/Al_2O_3$ on TiN-coated Si confirm the existence of interfacial layers between trilayer structures of $Al_2O_3/HfO_2/Al_2O_3$ after 600°C post-annealing. The memory units of $Pt/Al_2O_3/HfO_2/Al_2O_3/TiN/Si$ exhibit a typical bipolar, reliable, and reproducible resistive switching behavior, such as stable resistance ratio (>10) of OFF/ON states, sharp distribution of set and reset voltages, better switching endurance up to 10^3 cycles, and longer data retention at 85°C over 10 years. The possible switching mechanism of trilayer structure of $Al_2O_3/HfO_2/Al_2O_3$ has been proposed. The trilayer structure device units of $Al_2O_3/HfO_2/Al_2O_3$ on TiN-coated Si prepared by ALD may be a potential candidate for oxide-based resistive random access memory.

Keywords: Non-volatile memory; Atomic layer deposition; Resistance random access memory; Trilayer structure

Background

With traditional memories approaching their scaling limit, new memory concepts and materials in ultra-large-scale integration have drawn much attention. Resistive random access memory (RRAM) is one of the most promising candidates for next-generation non-volatile memory applications due to its simple structure, low power consumption, high-speed operation, nondestructive readout, and high-density integration [1]. Many semiconducting and insulating materials including binary transition metal oxides, perovskite oxides, chalcogenides, sulfides, amorphous silicon, organic materials, and ferroelectric materials have been investigated extensively for RRAM applications [2], especially metal oxides such as $Pr_{1-x}Ca_xMnO_3$ [3,4], $SrZrO_3$ [5], STO [6], Nb_2O_5 [7], NiO [8], ZrO_2 [9], SiO_2 [10], WO_3 [11], TiO_2 [12,13], Al_2O_3 [14], ZnO [15], and HfO_2 [16-18].

However, devices using metal oxides suffer from the dispersion of resistive switching parameters, such as the resistance values of low and high resistance states (LRS and HRS), the required set voltages from the HRS to the LRS, and reset voltages from the LRS to the HRS, which may lead to false programming and readout error [19]. Ruptures of the conducting filaments with various sizes at random locations are thought as the main reason for the non-uniformity of resistive switching parameters [20,21]. Several methods have been attempted to solve this problem, such as minimizing grain boundaries, doping, embedding nanoparticles, device area scaling, and bilayer structures in the memory devices [22-28]. The bilayer structure devices have been confirmed with evidently improved resistive switching behaviors [24,25]. Several models have been proposed to explain the enhanced performance [29,30]. Moreover, shrinkage of the active memory unit area to sub-100-nm size using a plug-contact-type bottom electrode was also able to obtain a sharp distribution in switching parameters.

The atomic layer deposition (ALD) is a kind of unique and modified chemical vapor deposition (CVD) method [31,32]. The precursor vapors are pulsed into the reactor alternatively and separated by purging with an inert gas.

* Correspondence: adli@nju.edu.cn
[1]National Laboratory of Solid State Microstructures and Department of Materials Science and Engineering, College of Engineering and Applied Sciences, Collaborative Innovation Center of Advanced Microstructures, Nanjing University, 22 Hankou Road, Nanjing 210093, People's Republic of China
Full list of author information is available at the end of the article

This results in a stepwise surface-saturated and self-limiting gas-solid reaction mechanism with many advantages such as good reproducibility, excellent conformity and uniformity over large area, low deposition temperature, and simple and precise control of film thickness, especially for deposition of nano-laminated structure. In this work, we fabricated trilayer-structure flexible RRAM units based on $Al_2O_3/HfO_2/Al_2O_3$ functional stacks on TiN-coated Si substrate by ALD so as to achieve excellent resistive switching performances with negligible parameter dispersion.

Methods

ALD was performed in a commercial Picosun SUNALE™ R-200 advanced reactor (Picosun, Masalantie 365, FI-02430 Masala, Finland). P-type Si (100) wafers with a resistivity of $1 \sim 10\ \Omega \cdot cm$ were used as the starting substrates. After the conventional RTA cleaning of the Si wafers without removing native oxide with the diluted HF solution, 30-nm-thick TiN was deposited on Si as bottom electrode at 400°C using $TiCl_4$ at room temperature (RT) and NH_3 plasma gas as the Ti and N sources by plasma-enhanced atomic layer deposition (PEALD). Liquid NH_3 at room temperature was used as NH_3 plasma source. The plasma power and NH_3 gas flow rate were 2,500 W and 150 sccm, respectively. Subsequently, 6 nm Al_2O_3/10 nm HfO_2/3 nm Al_2O_3 stacking structures (Figure 1a) were deposited in turn on TiN-coated Si substrates at 250°C by thermal ALD using $Hf[N(C_2H_5)CH_3]_4$ (TEMAH), $Al(CH_3)_3$, and H_2O as the Hf, Al, and O sources, respectively, where one oxide cycle consisted of 0.1-s metal source injection, 4-s N_2 purging, 0.1-s H_2O injection, and 4-s N_2 purging. TEMAH was evaporated at 150°C. Pure N_2 (99.999%) was used as carrier gas and purge gas. Then, 100-nm-thick Pt top electrodes were DC sputtered through a shadow mask with a diameter of 150 μm using the Q150T system. Post-metallization annealing (PMA) was performed at 600°C for 60 s in N_2 using rapid thermal annealing so as to remove slight organic residue in oxide stacking and improve the ohmic contact between the electrodes and metal oxide films.

The growth per cycle (GPC) of pure Al_2O_3 or HfO_2 on Si was determined by spectroscopic ellipsometer (GES-5, Annecy-le-Vieux, France). The nominal thickness of $Al_2O_3/HfO_2/Al_2O_3$ trilayer structure by ALD on TiN-coated Si was evaluated to be about 6.1, 10.3, and 3.0 nm, respectively. The actual thickness and microstructures of $Al_2O_3/HfO_2/Al_2O_3$ on TiN-coated Si were examined by a transmission electron microscope (TEM, Tecnai G2F20 S-Twin, FEI, Hillsboro, OR, USA) operating at 200 kV. The composition and chemical state of the samples were analyzed via X-ray photoelectron spectroscopy (XPS, Thermo Fisher K-Alpha, Thermo Fisher Scientific, Waltham, MA, USA) with a monochromatic Al K_α source ($h\nu$ = 1,486.6 eV) for excitation of photoelectrons. The charge effects were calibrated by setting the C 1-s photoemission at 284.6 eV. The XPS depth profile of $Al_2O_3/HfO_2/Al_2O_3$ on TiN-coated Si was obtained by Ar ion etching. The resistive switching properties were measured under different modes using a Keithley 4200-SCS semiconductor characterization system at room temperature and 85°C. A current compliance of 10 mA was imposed to protect the fabricated device units from damages of high currents during set processes.

Results and discussion

The schematic of the RRAM device structures of $Al_2O_3/HfO_2/Al_2O_3$ trilayer structure by ALD on TiN-coated

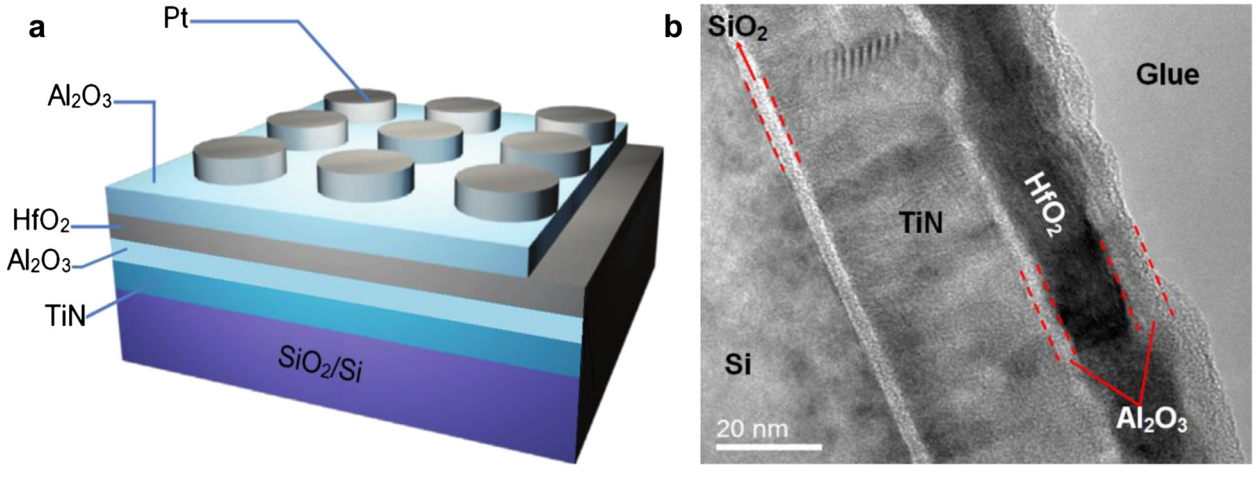

Figure 1 RRAM device structures and device unit of $Al_2O_3/HfO_2/Al_2O_3$ trilayer structure. (a) Schematic and test configuration of the RRAM device structures of $Al_2O_3/HfO_2/Al_2O_3$ trilayer structure on TiN-coated Si with Pt top electrode. **(b)** Typical cross-sectional TEM image of the device unit of $Al_2O_3/HfO_2/Al_2O_3$ trilayer structure on TiN-coated Si by ALD.

Si with Pt top electrode is illustrated in Figure 1a. Figure 1b shows the typical cross-sectional TEM image of the device unit. The laminated structures of $Al_2O_3/HfO_2/Al_2O_3/TiN/Si$ have been recognized clearly with the native oxide layer of SiO_2 between TiN and Si substrate. The measured average thickness of $Al_2O_3/HfO_2/Al_2O_3/TiN/SiO_2$ on Si is 6.1, 13.0, 3.0, 30.2, and 3.3 nm, respectively, which is basically consistent with the prescribed ones. After 600°C PMA, the partial and complete crystallization in TiN bottom electrode and HfO_2 interlayer with two Al_2O_3 amorphous layers is observed, respectively. Meanwhile, the $Al_2O_3/HfO_2/Al_2O_3$ trilayer structure on TiN-coated Si shows relatively rough interface and surface due to the crystallization of HfO_2 and TiN interlayers or possible interfacial diffusion between various layers at 600°C.

Figure 2 shows the XPS depth profile of $Al_2O_3/HfO_2/Al_2O_3$ on TiN-coated Si by Ar ion etching. The trilayer structure of $Al_2O_3/HfO_2/Al_2O_3$ on TiN-coated Si can be seen. Moreover, the significant interfacial diffusion between Al_2O_3/HfO_2 and Al_2O_3/TiN has been also confirmed, in good agreement with the TEM cross-sectional image. In spite of this, the memory units of $Al_2O_3/HfO_2/Al_2O_3$ trilayer structure on TiN-coated Si have been fabricated by ALD successfully.

The I-V curves of the device unit of $Pt/Al_2O_3/HfO_2/Al_2O_3/TiN/Si$ with various cycles are plotted in Figure 3a, indicating a typical bipolar resistive switching characteristic. For almost all the samples, larger forming voltage is needed to form conductive channels before the switching test. The forming voltage of device unit is about −2 V. The initial resistance state of the memory unit in the first cycle (black curve) is higher than that of the second and third cycles (blue and red curves). Moreover, as-prepared original device unit is in the LRS and an excess positive voltage of 2 V is needed to reset the device unit from LRS to HRS (denoted by arrows 1 and 2 in Figure 3a). The I-V curves from the second and third cycles are almost in superposition with similar set and reset voltages.

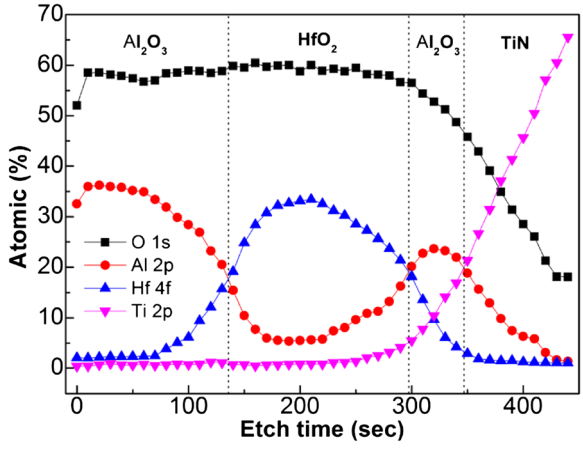

Figure 2 XPS depth profile of $Al_2O_3/HfO_2/Al_2O_3$ on TiN-coated Si by Ar ion etching.

For high-density memory application, uniformity of both set and reset voltages is very important. Figure 3b,c plots the statistical results of distribution and cumulative probability of the set and reset voltages measured from a single device unit for 400 times tests. The set and reset voltages show narrow distribution from −1.21 to −0.85 V and from 1.24 to 1.38 V in a device unit, respectively. Their corresponding average values are −0.96 and 1.31 V, respectively. Moreover, 50 randomly selected device units also exhibit less deviation of set and reset voltages, as seen in Figure 3d. Especially, the reset voltage has better monodispersion than the set voltage in Figure 3b-d.

The switching endurance and data retention characteristics of the device unit of $Pt/Al_2O_3/HfO_2/Al_2O_3/TiN/Si$ have been examined. The stable and reproducible switching properties have been achieved in Figure 4a,b. The sweeping voltage was applied from 0 to −2 V for set and 0 to 1.5 V for reset with a reading voltage of 0.1 V at room temperature. The endurance test shows a consistent 10^3 switching cycle with a stable resistance ratio of OFF/ON states above 10 (Figure 4a). Retention characteristics of the device unit were measured at room temperature and 85°C, as seen in Figure 4b. Both HRS and LRS were read at 0.1 V for cumulative waiting time of 10^4 s. At room temperature, no obvious degradation of the memory window is observed with slightly increasing LRS and HRS. At 85°C, the memory window exhibits better thermal stability with the resistance ratio of LRS/HRS >10, indicating a better retention endurance of the memory unit over a 10-year lifetime based on the extrapolation method. It is interesting that in the retention test, both HRS and LRS increase with time at room temperature but decrease at 85°C on the contrary. This phenomenon can be explained by the change of oxygen vacancy concentration with time at room temperature and 85°C. As known, the oxygen vacancy concentration of some oxide thin film samples stored in air ambient is not constant [33]. The air oxygen may slowly diffuse into the $Al_2O_3/HfO_2/Al_2O_3$-based samples at room temperature, leading to the gradual decrease of oxygen vacancy concentration, i.e. the increase of HRS and LRS in oxide thin films with retention time. When raising the measuring temperature to 85°C, on one hand, the oxygen diffusion into the device unit reduces the oxygen vacancy concentration; on the other hand, the enhanced temperature may produce more oxygen vacancies in $Al_2O_3/HfO_2/Al_2O_3$ trilayer structures. Evidently the increased carriers of oxygen vacancies predominate, so both HRS and LRS of the device unit decrease with time at 85°C.

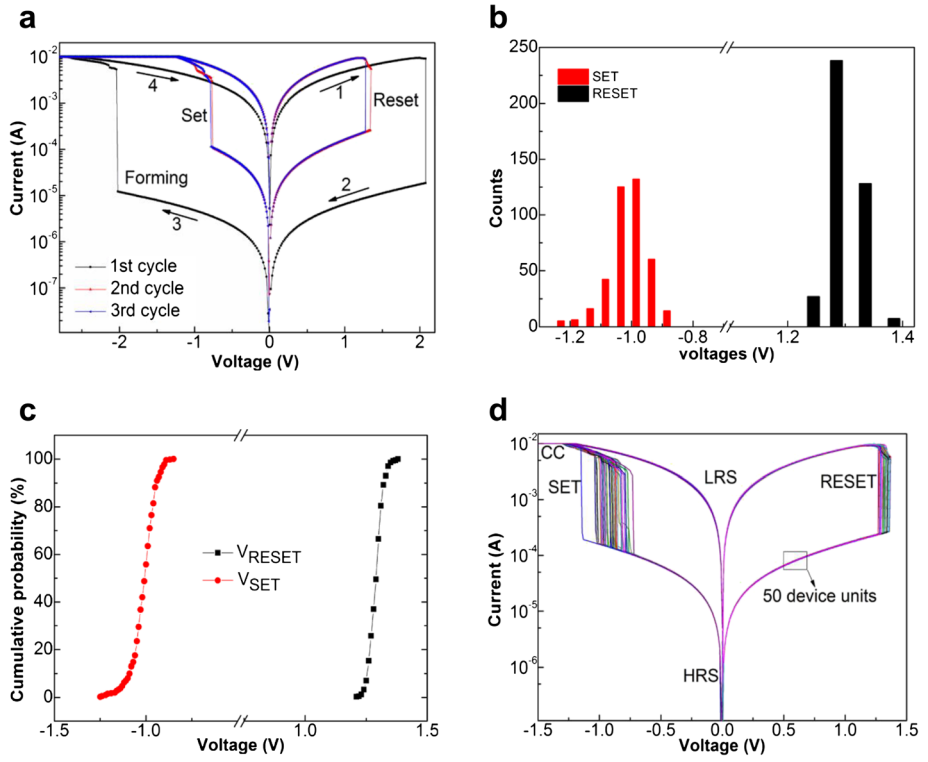

Figure 3 Resistive switching characteristics of the device unit and distribution of the set and reset voltages. (a) Typical resistive switching characteristics of the device unit of $Pt/Al_2O_3/HfO_2/Al_2O_3/TiN/Si$ after initial, second, and third cycles. **(b, c)** Statistical results of distribution and cumulative probability of the set and reset voltages measured from a device unit for 400 times tests. **(d)** Resistive switching data of 50 randomly selected device units.

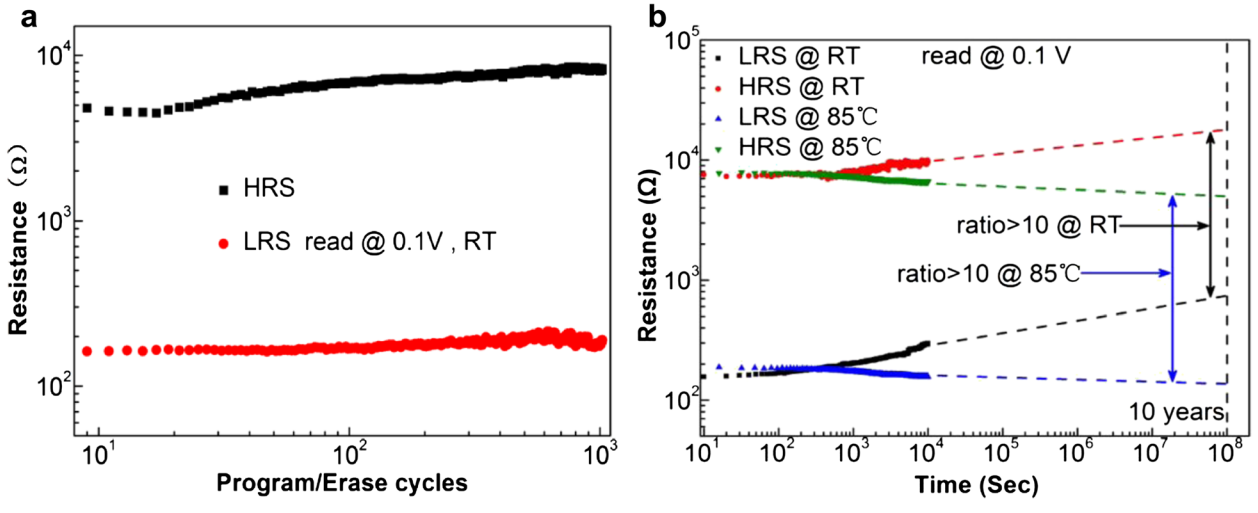

Figure 4 The durability of the device unit of $Pt/Al_2O_3/HfO_2/Al_2O_3/TiN/Si$. (a) The continuous program and erase test. **(b)** Read disturbance test for device after 10^4-s retention time at room temperature and 85°C.

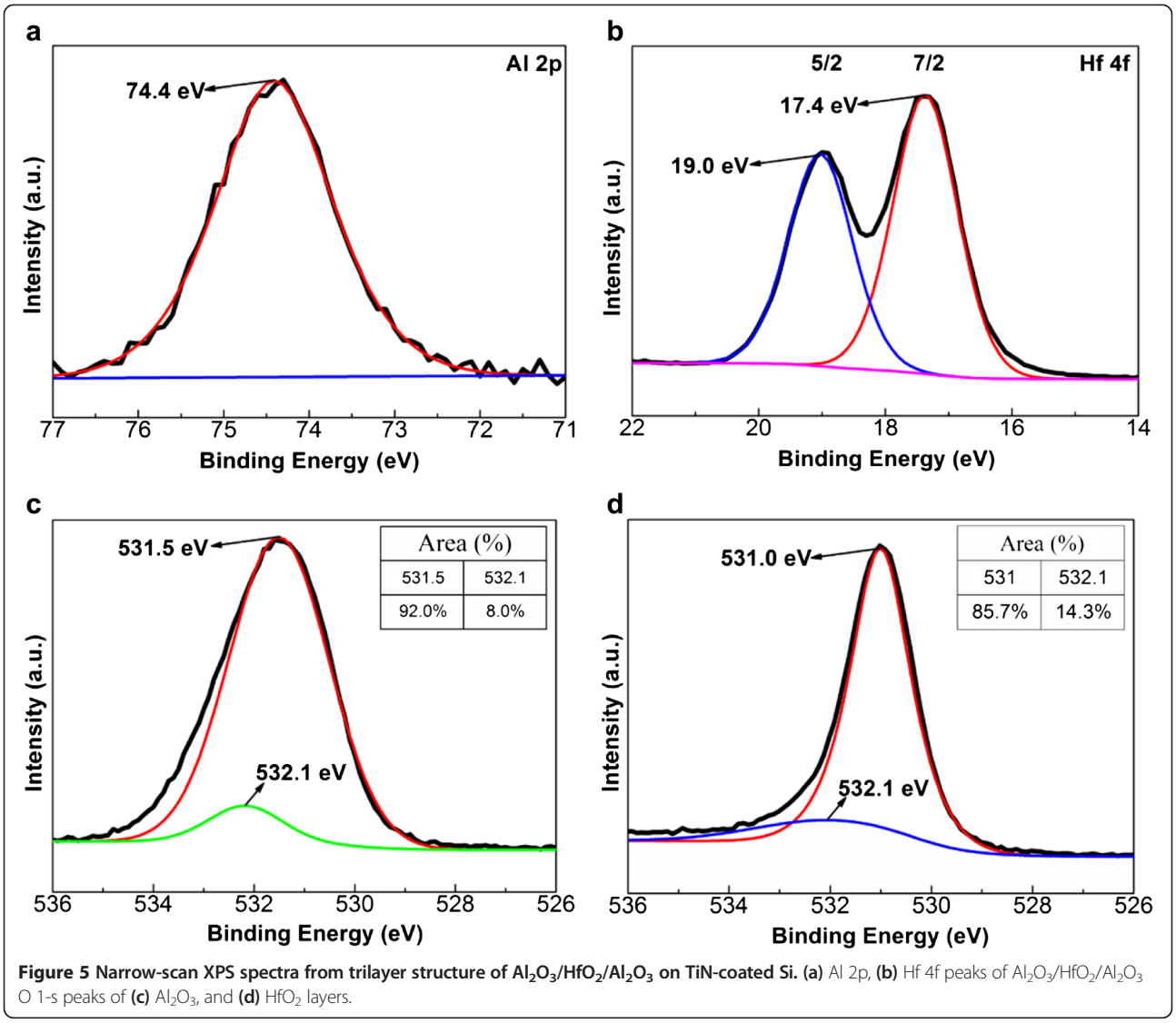

Figure 5 Narrow-scan XPS spectra from trilayer structure of $Al_2O_3/HfO_2/Al_2O_3$ on TiN-coated Si. (a) Al 2p, **(b)** Hf 4f peaks of $Al_2O_3/HfO_2/Al_2O_3$ O 1-s peaks of **(c)** Al_2O_3, and **(d)** HfO_2 layers.

Evidently, the above results confirm that the device unit of trilayer structure of $Al_2O_3/HfO_2/Al_2O_3$ on TiN-coated Si exhibits excellent resistive switching performances, such as stability of resistance ratio of on/off states, uniformity of set and reset voltages, and reliability and durability of switching between the LRS and the HRS.

In order to obtain in-depth understanding on switching mechanism of trilayer structure of $Al_2O_3/HfO_2/Al_2O_3$ on TiN-coated Si, we performed the XPS analyses on $Al_2O_3/HfO_2/Al_2O_3$ structures. XPS spectra were fitted with Gaussian-Lorentzian (G-L) functions after smart-type background subtraction.

The narrow-scan XPS spectra of Al 2p, Hf 4f, and O 1-s peaks in Al_2O_3 and HfO_2 layers are shown in Figure 5a-d. The Al 2p peak is located at 74.4 eV, which is assigned to Al-O bonding. The Hf $4f_{5/2}$ and Hf $4f_{7/2}$ peaks at 19.0 and 17.4 eV with a spin-orbit splitting of 1.6 eV are consistent with the literature data of high k HfO_2/Si [34]. The O 1-s spectra from Al_2O_3 and HfO_2 layers can be deconvoluted into two peaks in Figure 5c,d. The slightly lower binding energies of the O 1-s peak at around 531.5 and 531.0 eV, which correspond to Al-O and Hf-O bonding in Al_2O_3 and HfO_2 layers, respectively. Whereas the slightly higher energy of 532.1 eV in the O 1-s spectra of Figure 5c, d is attributed to the oxygen vacancies in Al_2O_3 and HfO_2 layers based on the literature reports [35,36]. The inset tables in Figure 5c, d list the area proportion of each peak. The percentage of oxygen vacancies in the Al_2O_3 and HfO_2 layer is about 8.0% and 14.3%, respectively. Evidently, the oxygen vacancy concentration of HfO_2 is higher than that of Al_2O_3. The TEM and XPS depth results of trilayer structure of $Al_2O_3/HfO_2/Al_2O_3$ confirm the existence of significant interfacial

diffusion between Al_2O_3 and HfO_2 films. Defect equation of the interfacial diffusion can be expressed as:

$$Al_2O_3 \xrightarrow{HfO_2} 2Al'_{Hf} + 3O_O^{\times} + V_O^{\cdot\cdot} \quad (1)$$

$$HfO_2 \xrightarrow{Al_2O_3} 2Hf^{\cdot}_{Al} + 2O_O^{\times} + O_i'' \quad (2)$$

Where Al'_{Hf} means that Al^{3+} occupies the position of Hf^{4+} in HfO_2 lattice, with singular negative charge. $V_O^{\cdot}$ refers to oxygen vacancy with double positive charge in oxide lattice. $Hf^{\cdot}_{Al}$ means that Hf^{4+} occupies the position of Al^{3+} in Al_2O_3 lattice, with singular positive charge. O_i'' means oxygen anion on an interstitial site, with double negative charge. $O_O^{\times}$ represents the neutral oxygen atom in an oxide lattice site.

Therefore, based on Equations 1 and 2, HfO_2 layer produces and stores more oxygen vacancies than Al_2O_3 layer. The physical size of the conductive filament in oxygen vacancy-deficient layer is narrower than in the oxygen vacancy-rich layer [19], so it can be inferred reasonably that the filament in HfO_2 layer is thicker and more intensive. Based on the bilayer-structure model, the oxygen exchange through the interface between two layers played an important role in improving resistive switching characteristics [19]. In this work, the two interfacial layers (IL) between trilayer-structure of $Al_2O_3/HfO_2/Al_2O_3$ on TiN-coated Si have also a similar effect on connected or broken filaments in memory units, as indicated in Figure 6a,b.

The two interfacial layers between Al_2O_3/IL/HfO_2/IL/Al_2O_3 could affect the growth position, direction, and overlapping of conductive filaments. The linkage (Figure 6a) or rupture (Figure 6b) of the conductive filaments corresponds to the SET from HRS to LRS or the RESET from LRS to HRS, respectively, which more easily occur in two interfacial layers. Further, the shape and position of the conductive filaments in Al_2O_3 and HfO_2 layers change less in the SET and RESET processing. The resistive switching mechanism is mainly dominated by formation and rupture of conducting filaments of oxygen vacancies in interfacial layers. The thermal redox near the interface between the oxides or electrochemical migration of oxygen ions may be also the main driving force [4,37,38]. Further work is needed to understand this mechanism well.

Conclusions

In summary, reliable and uniform RRAM units based on trilayer structure of $Al_2O_3/HfO_2/Al_2O_3$ on TiN-coated Si have been prepared by ALD. The cross-sectional HRTEM image and XPS depth profile of $Al_2O_3/HfO_2/Al_2O_3$ on TiN-coated Si confirm the existence of interfacial layers between the trilayer structure of $Al_2O_3/HfO_2/Al_2O_3$. The memory units of Pt/Al_2O_3/HfO_2/Al_2O_3/TiN/Si exhibit a typical bipolar, reliable, and reproducible resistive switching behavior, such as stable resistance ratio (>10) of OFF/ON states, sharp distribution of set and reset voltages, better switching endurance up to 10^3 cycles, and longer data retention at 85°C over 10 years. The possible switching mechanism of trilayer structure of $Al_2O_3/HfO_2/Al_2O_3$ has been proposed, and two interfacial layers between Al_2O_3/IL/HfO_2/IL/Al_2O_3 play an important role in improving resistive switching characteristics. The oxygen ion migration and the redox reactions at the tip of the localized filament lead to the formation/rupture of the conducting filaments mainly in two interfacial layers during the SET and RESET processing. The $Al_2O_3/HfO_2/Al_2O_3$ trilayer structure device units by ALD may be a potential candidate for oxide-based RRAM.

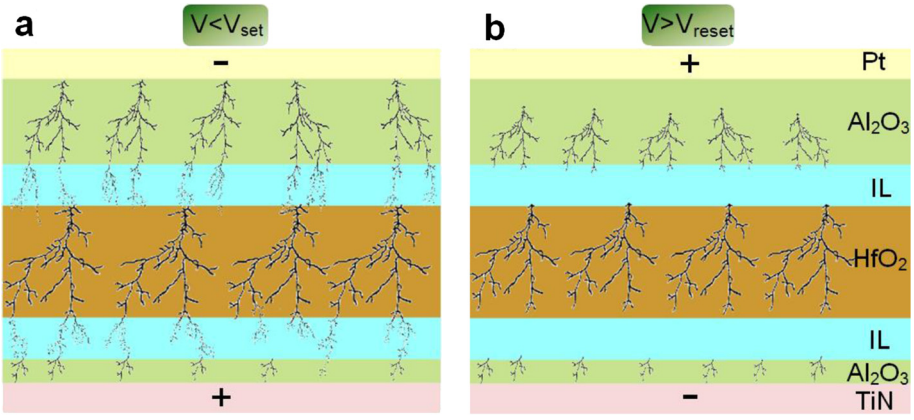

Figure 6 Schematics of proposed filament-switching mechanism of Pt/Al_2O_3/HfO_2/Al_2O_3 on TiN-coated Si. (a) Low resistance state (LRS) when applied voltage is less than set voltage. **(b)** High resistance state (HRS) when applied voltage is greater than reset voltage.

Competing interests
The authors declare that they have no competing interests.

Authors' contributions
LGW carried out the sample fabrication and device measurements and drafted the manuscript. LGW and YQC did the data analysis and interpreted the results. XQ and YQC helped to finish TEM sample preparation and observation. ADL, DW, and GYF participated in the discussion of results. ADL supervised the whole work and revised the manuscript. All authors read and approved the final manuscript.

Acknowledgements
This project is supported by the Natural Science Foundation of China (51202107), a grant from the State Key Program for Basic Research of China (2015CB921203 and 2011CB922104). ADL also thanks the support of Priority Academic Program Development in the Jiangsu Province, Open Project of National Laboratory of Solid State Microstructures (M27001), and the Doctoral Fund of Ministry of Education of China (20120091110049). Dr. Han-Ni Xu was acknowledged for her help in TEM observation.

Author details
[1]National Laboratory of Solid State Microstructures and Department of Materials Science and Engineering, College of Engineering and Applied Sciences, Collaborative Innovation Center of Advanced Microstructures, Nanjing University, 22 Hankou Road, Nanjing 210093, People's Republic of China. [2]Anhui Key Laboratory of Functional Coordination Compounds, School of Chemistry and Chemical Engineering, Anqing Normal University, 128 Linghu South Road, Anhui 246011, People's Republic of China.

Received: 15 November 2014 Accepted: 2 March 2015
Published online: 19 March 2015

References

1. Li Y, Long S, Lv H, Liu Q, Wang Y, Zhang S, et al. Improvement of resistive switching characteristics in ZrO_2 film by embedding a thin TiO_x layer. Nanotechnology. 2011;22:254028.
2. Yang JJ, Strukov DB, Stewart DR. Memristive devices for computing. Nat Nanotechnol. 2013;8:13–24.
3. Zhuangl WW, Pan W, Ulrich BD, Lee JJ, Stecker L, Burmaster A, et al. Novel colossal magnetoresistive thin film nonvolatile resistance random access memory (RRAM). IEEE Electron Device Lett. 2002;23:193–5.
4. Fujimoto M, Koyama H, Kobayashi S, Tamai Y, Awaya N, Nishi Y, et al. Resistivity and resistive switching properties of $Pr_{0.7}Ca_{0.3}MnO_3$ thin films. Appl Phys Lett. 2006;89:243504.
5. Liu C-Y, Wu P-H, Wang A, Jang W-Y, Young J-C, Chiu K-Y, et al. Bistable resistive switching of a sputter-deposited Cr-doped $SrZrO_3$ memory film. IEEE Electron Device Lett. 2005;26:351–3.
6. Szot K, Speier W, Bihlmayer G, Waser R. Switching the electrical resistance of individual dislocations in single-crystalline $SrTiO_3$. Nat Mater. 2006;5:312–20.
7. Sim H, Choi D, Lee D, Seo S, Lee M-J, Yoo I-K, et al. Resistance-switching characteristics of polycrystalline Nb_2O_5 for nonvolatile memory application. IEEE Electron Device Lett. 2005;26:292–5.
8. Seo S, Lee MJ, Seo DH, Jeoung EJ, Suh DS, Joung YS, et al. Reproducible resistance switching in polycrystalline NiO films. Appl Phys Lett. 2004;85:5655.
9. Lee D, Choi H, Sim H, Choi D, Hwang H, Lee M-J, et al. Resistance switching of the nonstoichiometric zirconium oxide for nonvolatile memory applications. IEEE Electron Device Lett. 2005;26:719–23.
10. Schindler C, Weides M, Kozicki MN, Waser R. Low current resistive switching in Cu-SiO_2 cells. Appl Phys Lett. 2008;92:122910.
11. Kozicki MN, Gopalan C, Balakrishnan M, Mitkova M. A low-power nonvolatile switching element based on copper-tungsten oxide solid electrolyte. IEEE Trans Nanotechnol. 2006;5:535–44.
12. Fujimoto M, Koyama H, Konagai M, Hosoi Y, Ishihara K, Ohnishi S, et al. TiO_2 anatase nanolayer on TiN thin film exhibiting high-speed bipolar resistive switching. Appl Phys Lett. 2006;89:223509.
13. Fujimoto M, Koyama H, Hosoi Y, Ishihara K, Kobayashi S. High-speed resistive switching of TiO_2/TiN nano-crystalline thin film. Jpn J Appl Phys. 2006;45:310–2.
14. Chen L, Xu Y, Sun QQ, Liu H, Gu JJ, Ding SJ, et al. Highly uniform bipolar resistive switching with Al_2O_3 buffer layer in robust NbAlO-based RRAM. IEEE Electron Device Lett. 2010;31:356–8.
15. Chang W-Y, Lai Y-C, Wu T-B, Wang S-F, Chen F, Tsai M-J. Unipolar resistive switching characteristics of ZnO thin films for nonvolatile memory applications. Appl Phys Lett. 2008;92:022110.
16. Chen YS, Lee HY, Chen PS, Tsai CH, Gu PY, Wu TY, et al. Challenges and opportunities for HfO_x based resistive random access memory. IEEE International Electron Devices Meeting. 2011;31:31.3.1–3.4.
17. Lee HY, Chen PS, Wu TY, Wang CC, Tzeng PJ, Lin CH, et al. Electrical evidence of unstable anodic interface in Ru/HfO_x/TiN unipolar resistive memory. Appl Phys Lett. 2008;92:142911.
18. Walczyk C, Wenger C, Sohal R, Lukosius M, Fox A, Dąbrowski J, et al. Pulse-induced low-power resistive switching in HfO_2 metal-insulator-metal diodes for nonvolatile memory applications. J Appl Phys. 2009;105:114103.
19. Lee J, Bourim EM, Lee W, Park J, Jo M, Jung S, et al. Effect of ZrO_x/HfO_x bilayer structure on switching uniformity and reliability in nonvolatile memory applications. Appl Phys Lett. 2010;97:172105.
20. Waser R, Dittmann R, Staikov G, Szot K. Redox-based resistive switching memories - nanoionic mechanisms, prospects, and challenges. Adv Mater. 2009;21:2632–63.
21. Pan F, Gao S, Chen C, Song C, Zeng F. Recent progress in resistive random access memories: materials, switching mechanisms, and performance. Mater Sci Eng R Rep. 2014;83:1–59.
22. Yoon J, Choi H, Lee D, Park J-B, Lee J, Seong D-J, et al. Excellent switching uniformity of Cu-doped MoO_x/GdO_x bilayer for nonvolatile memory applications. IEEE Electron Device Lett. 2009;30:457–9.
23. Lin M-H, Wu M-C, Huang C-Y, Lin C-H, Tseng T-Y. High-speed and localized resistive switching characteristics of double-layer $SrZrO_3$ memory devices. J Phys D Appl Phys. 2010;43:295404.
24. Cheng CH, Chin A, Yeh FS. Ultralow-power Ni/GeO/STO/TaN resistive switching memory. IEEE Electron Device Lett. 2010;31:1020–2.
25. Terai M, Sakotsubo Y, Kotsuji S, Hada H. Resistance controllability of Ta_2O_5/TiO_2 stack ReRAM for low-voltage and multilevel operation. IEEE Electron Device Lett. 2010;31:204–6.
26. Morrison FD, Sinclair DC, West AR. Characterization of lanthanum-doped barium titanate ceramics using impedance spectroscopy. J Am Ceram Soc. 2001;84:531–8.
27. Fang R-C, Sun Q-Q, Zhou P, Yang W, Wang P-F, Zhang DW. High-performance bilayer flexible resistive random access memory based on low-temperature thermal atomic layer deposition. Nanoscale Res Lett. 2013;8:1–7.
28. Kim I, Koo J, Lee J, Jeon H. A comparison of Al_2O_3/HfO_2 and Al_2O_3/ZrO_2 bilayers deposited by the atomic layer deposition method for potential gate dielectric applications. Jpn J Appl Phys. 2006;45:919–25.
29. Sun Q-Q, Gu J-J, Chen L, Zhou P, Wang P-F, Ding S-J, et al. Controllable filament with electric field engineering for resistive switching uniformity. IEEE Electron Device Lett. 2011;32:1167–9.
30. Song YL, Liu Y, Wang YL, Wang M, Tian XP, Yang LM, et al. Low reset current in stacked AlO_x/WO_x resistive switching memory. IEEE Electron Device Lett. 2011;32:1439–41.
31. Puurunen RL. Surface chemistry of atomic layer deposition: a case study for the trimethylaluminum/water process. J Appl Phys. 2005;97:121301.
32. Sherman A. Atomic layer deposition for nanotechnology: an enabling process for nanotechnology fabrication. New York: Ivoryton Press; 2008.
33. Zhang S-T, Yuan G-L, Wang J, Chen Y-F, Cheng G-X, Liu Z-G. Temperature-dependent effect of oxygen vacancy on polarization switching of ferroelectric $Bi_{3.25}La_{0.75}Ti_3O_{12}$ thin films. Solid State Commun. 2004;132:315–8.
34. Moulder JF, Stickle WF, Sobol PE, Bomben KD. Handbook of X-ray photoelectron spectroscopy. In: Chastain J, King RC, editors. Physical electronics, Minnesota. 2nd ed. 1995. p. 44–5.
35. Dupin J-C, Gonbeau D, Vinatier P, Levasseur A. Systematic XPS studies of metal oxides, hydroxides and peroxides. PCCP. 2000;2:1319–24.
36. Huang C-Y, Huang C-Y, Tsai T-L, Lin C-A, Tseng T-Y. Switching mechanism of double forming process phenomenon in ZrO_x/HfO_y bilayer resistive switching memory structure with large endurance. Appl Phys Lett. 2014;104:062901.

37. Kinoshita K, Tamura T, Aoki M, Sugiyama Y, Tanaka H. Bias polarity dependent data retention of resistive random access memory consisting of binary transition metal oxide. Appl Phys Lett. 2006;89:103509.
38. Kim KM, Choi BJ, Hwang CS. Localized switching mechanism in resistive switching of atomic-layer-deposited TiO_2 thin films. Appl Phys Lett. 2007;90:242906.